Journal of Applied Physics

RESEARCH ARTICLE | DECEMBER 23 2024

Eliminating resistance measurement error due to thermoelectric effects in micro four-point probe measurements

Neetu Lamba ; Benny Guralnik ; Jesús Prado-Gonjal; Anthony V. Powell ; Nini Pryds ; Ole Hansen ; Dirch H. Petersen ; Braulio Beltrán-Pitarch

J. Appl. Phys. 136, 244501 (2024)
https://doi.org/10.1063/5.0244261

Articles You May Be Interested In

Advanced carrier depth profiling on Si and Ge with micro four-point probe

J. Vac. Sci. Technol. B (January 2008)

Note: A simple approach to fabricate a microscopic four-point probe for conductivity measurements in ultrahigh vacuum

Rev. Sci. Instrum. (July 2013)

Development of a surface conductivity measurement system for ultrahigh vacuum transmission electron microscope

Rev. Sci. Instrum. (November 2009)

08 January 2025 14:24:06

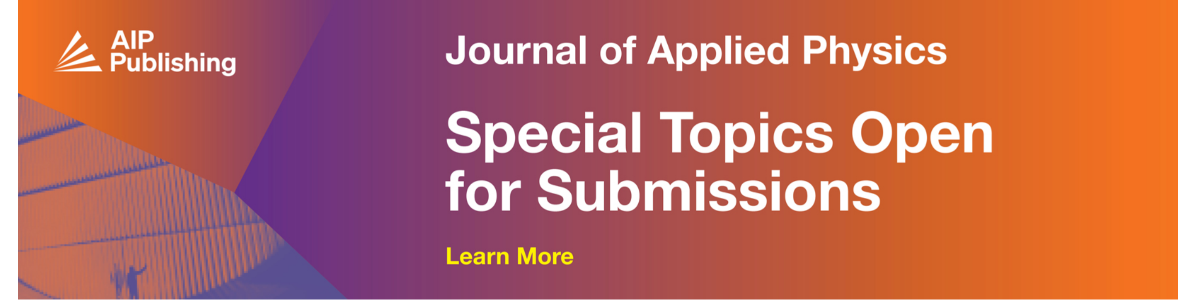

Journal of Applied Physics | METHOD | pubs.aip.org/aip/jap

Eliminating resistance measurement error due to thermoelectric effects in micro four-point probe measurements

Cite as: J. Appl. Phys. 136, 244501 (2024); doi: 10.1063/5.0244261
Submitted: 17 October 2024 · Accepted: 5 December 2024 ·
Published Online: 23 December 2024

View Online

Export Citation

CrossMark

Neetu Lamba,[1] Benny Guralnik,[2] Jesús Prado-Gonjal,[3,4] Anthony V. Powell,[3] Nini Pryds,[1] Ole Hansen,[5] Dirch H. Petersen,[1] and Braulio Beltrán-Pitarch[1,2,a)]

AFFILIATIONS

[1]DTU Energy—Department of Energy Conversion and Storage, Technical University of Denmark, Fysikvej 310, Kgs. Lyngby DK-2800, Denmark
[2]KLA Corporation, Diplomvej 373, Kgs Lyngby DK-2800, Denmark
[3]Department of Chemistry, University of Reading, Reading RG6 6AD, United Kingdom
[4]Departamento de Química Inorgánica, Universidad Complutense de Madrid, Ciudad Universitaria s/n, Madrid E-28040, Spain
[5]DTU Nanolab—National Centre for Nano Fabrication and Characterization, Technical University of Denmark, Ørsteds Plads 347, Kgs. Lyngby DK-2800, Denmark

[a)]**Author to whom correspondence should be addressed:** braulio.b.pitarch@ntnu.no

08 January 2025 14:24:06

ABSTRACT

The micro four-point probe (M4PP) technique has become a well-established method for characterizing the electrical properties of materials. However, extra attention must be paid when measuring the resistivity of thermoelectric materials due to the possibility of an additional Seebeck voltage. This issue vanishes when measuring at a sufficiently high frequency, but the threshold frequency is substantial due to the small separation between the pins of the probes. Typical M4PP measurements are far from reaching this frequency, and their accuracy on thermoelectric materials is severely compromised. In this work, we explain the experimental conditions needed to measure reliably the electrical conductivity of thermoelectric materials and present a new method for measuring this property that reduces the frequency requirements by two orders of magnitude. The method is proven using two skutterudites and bismuth telluride material. It is also found that the resistance overestimation in the bismuth telluride sample is larger than that in the skutterudites due to its superior thermoelectric properties; the overestimate reaching 35%. The advances reported here enable the M4PP technique to be used for the measurement of the electrical conductivity of thermoelectric materials.

© *2024 Author(s). All article content, except where otherwise noted, is licensed under a Creative Commons Attribution (CC BY) license (https://creativecommons.org/licenses/by/4.0/).* https://doi.org/10.1063/5.0244261

I. INTRODUCTION

Four-point techniques have been used to extract electrical properties for over a hundred years,[1] but only a quarter of a century has passed since they were developed for measuring at the microscopic scale.[2] The micro four-point probe (M4PP) method uses two small pins to pass an electric current through a sample and another pair of pins for recording a potential difference. Owing to its high precision and resolution, it has become an important tool for measuring several properties, including sheet resistance,[3,4] electron mobility,[5] carrier density,[5] and magnetoresistance.[6,7] In these applications, the measuring samples have poor thermoelectric properties, and the measured M4PP resistance has always been assumed to be free of error arising from the Peltier effect. Lately, however, the technique has also been proven useful for measuring thermoelectric and thermal properties, like the temperature coefficient of resistance,[8,9] the thermal boundary conductance,[9] the Seebeck over thermal conductivity ratio,[10,11] and the thermal diffusivity.[12,13] When measuring thermoelectric materials, errors in the measured M4PP resistance due to the Peltier effect may significantly compromise the accuracy of the method.

© Author(s) 2024

The presence of the Seebeck voltage originating from the Peltier effect has been extensively used for the measurement of thermoelectric properties since 1958 when Harman presented a method for measuring the thermoelectric figure of merit.[14] Advanced versions of the Harman method,[15,16] impedance spectroscopy,[17–20] and other four-point techniques[21,22] can be very fast and accurate, encouraging their widescale adoption. The working principle of all these methods consists of measuring at least two points at equilibrium. The first is by applying a sudden change in the measuring current (or measuring with an AC current at high frequency), which supplies the pure ohmic resistance of the sample. The second approach is the application of a DC (or an AC at low frequency), where a Seebeck voltage is added to the pure ohmic signal due to the generation of a temperature difference inside the sample caused by the Peltier effect. This second point requires a careful minimization of thermal losses to avoid underestimating the thermoelectric properties. The unaccounted thermal losses in experimental setups commonly reported in the literature too often contribute to a 30%–40% underestimation of the Seebeck voltage.[15,23] Therefore, it is reasonable to assume that typical M4PP systems, which measure at low frequency and are not designed for reducing thermal losses, measure only a fraction of the total thermoelectric signal. Considering that good thermoelectric materials can generate a Seebeck voltage exceeding the pure ohmic contribution and that this contribution is uncertain due to potentially severe thermal losses, it follows that the M4PP in its current form is not capable of accurately measuring the electrical resistivity of thermoelectric materials.

A solution for M4PP measurements to be error-free due to the Peltier effect is to perform the measurements at high frequency. However, the small distance between the pins (in the μm range) causes the required frequency to be large (up to a few GHz, as explained later in this paper), and both the small pin separation and the high measuring frequency may generate parasitic capacitive effects. Since measuring with smaller probes (and smaller distances between pins) increases the spatial resolution of the technique, a constant reduction in pin separation increases the need for alternative methods to determine the electrical resistivity without being forced to measure at the high-frequency limit. Here, we explain in detail the conditions that must be met to avoid introducing errors due to the Peltier effect in M4PP measurements and propose an analytical expression that can be used to calculate and reduce the required measuring frequency. This new theoretical model is then used to determine the electrical conductivity of two isotropic skutterudites and anisotropic bismuth telluride material.

II. THEORETICAL MODEL

As shown in Fig. 1(a), in an M4PP measurement, an AC with amplitude I_0 represented by $I = I_0 \sin(2\pi f t)$, where f is the frequency and t is the time, is passed through two electrodes placed on the surface of a sample. At both junctions between the pins and the sample, heat flux is generated due to the Peltier effect during one half-period and removed during the other half-period. When the temperature of the sample at the location of the voltage pins is changed by the Peltier effect, an additional voltage (more than the ohmic voltage drop) due to the Seebeck effect is generated. Therefore, the measured resistance for a given electrode separation, s, and intrinsic material properties is free of error induced by the Peltier effect only at high frequency. This is shown in Fig. 1(b), where simulations of the resistance (ratio of the in-phase voltage to current) normalized to their high-frequency limit are plotted for different s. The red crosses in Fig. 1(b) indicate a cutoff frequency $f_c = 2.25\pi D/s^2$ (where D is the thermal diffusivity of the measuring sample), which was defined as explained in the supplementary material. The dependency of the cutoff frequency on s and D is depicted in Fig. 1(c). It should be noted that the pin separation in commercial probes can be as small as 500 nm, and they are expected to shrink to improve spatial resolution. Hence, when measuring materials with larger thermal diffusivity, the required measuring frequency to avoid Peltier-induced errors could enter the GHz regime [see Fig. 1(c)].

The potential difference ${}^{uv}_{pq}\Delta V$ between pin p and pin q due to a current introduced at pin u and removed at pin v [see Fig. 1(a)] can be calculated using the superposition principle,

$$ {}^{uv}_{pq}\Delta V = {}^{u}_{p}\Delta V + {}^{v}_{p}\Delta V - {}^{u}_{q}\Delta V - {}^{v}_{q}\Delta V, \tag{1} $$

where ${}^{l}_{k}\Delta V$ is the potential at pin k due to the current imposed at pin l, which can be calculated as

$$ {}^{l}_{k}\Delta V(r_{k,l}, t) = \frac{I}{2\pi r_{k,l}\sigma} + \frac{\alpha^2 T I}{2\pi\kappa r_{k,l}} e^{-(1+i)\sqrt{\frac{\omega}{2D}}r_{k,l}}, \tag{2} $$

where $r_{k,l}$ is the distance between pins k and l, I is the current (positive at pin u and negative at pin v), σ is the electrical conductivity of the sample, α is its Seebeck coefficient, T is the ambient temperature, κ is the thermal conductivity, ω is the angular frequency ($\omega = 2\pi f$), and i is the imaginary unit. The first part of Eq. (2) is purely ohmic, while the second part is the Peltier contribution to the voltage. Notice that the latter is derived as described in the appendix of Ref. 12 by assuming a power amplitude of the Peltier heat ($\alpha T I$) giving rise to temperature fluctuations at an angular frequency ω instead of Joule heating coming from the contacts and fluctuating at the second harmonic (2ω).

Rearranging Eq. (2) considering that the sample can be anisotropic and that a significant amount of heat may be lost (primarily toward the current pins),

$$ {}^{l}_{k}\Delta V(r_{k,l}, t) = \frac{I}{2\pi r_{k,l}\sigma_{\text{eff}}}\left[1 + C e^{-(1+i)\sqrt{\frac{\omega}{2D_x}}r_{k,l}}\right], \tag{3} $$

leads to the definition of σ_{eff} as the effective electrical conductivity, C as a correction factor, and D_x as the thermal diffusivity in the probe direction [see Fig. 1(a)]. More information about σ_{eff} and D_x can be found in Ref. 13. It should be noted that C is simply the dimensionless figure of merit $ZT = \sigma\alpha^2 T/\kappa$, when measuring isotropic samples and neglecting the heat losses towards the current pins. Since heat losses are inevitable, C is less than ZT in practice and it defines the percentage of resistance overestimation when measuring at the low-frequency limit.

Equations (1) and (3) reveal that given the geometry and measuring frequency, only three parameters (D_x, σ_{eff}, and C) define the measured M4PP resistance. Since D_x can be measured from the second harmonic phase shift,[12,13] the remaining two parameters

08 January 2025 14:24:06

© Author(s) 2024

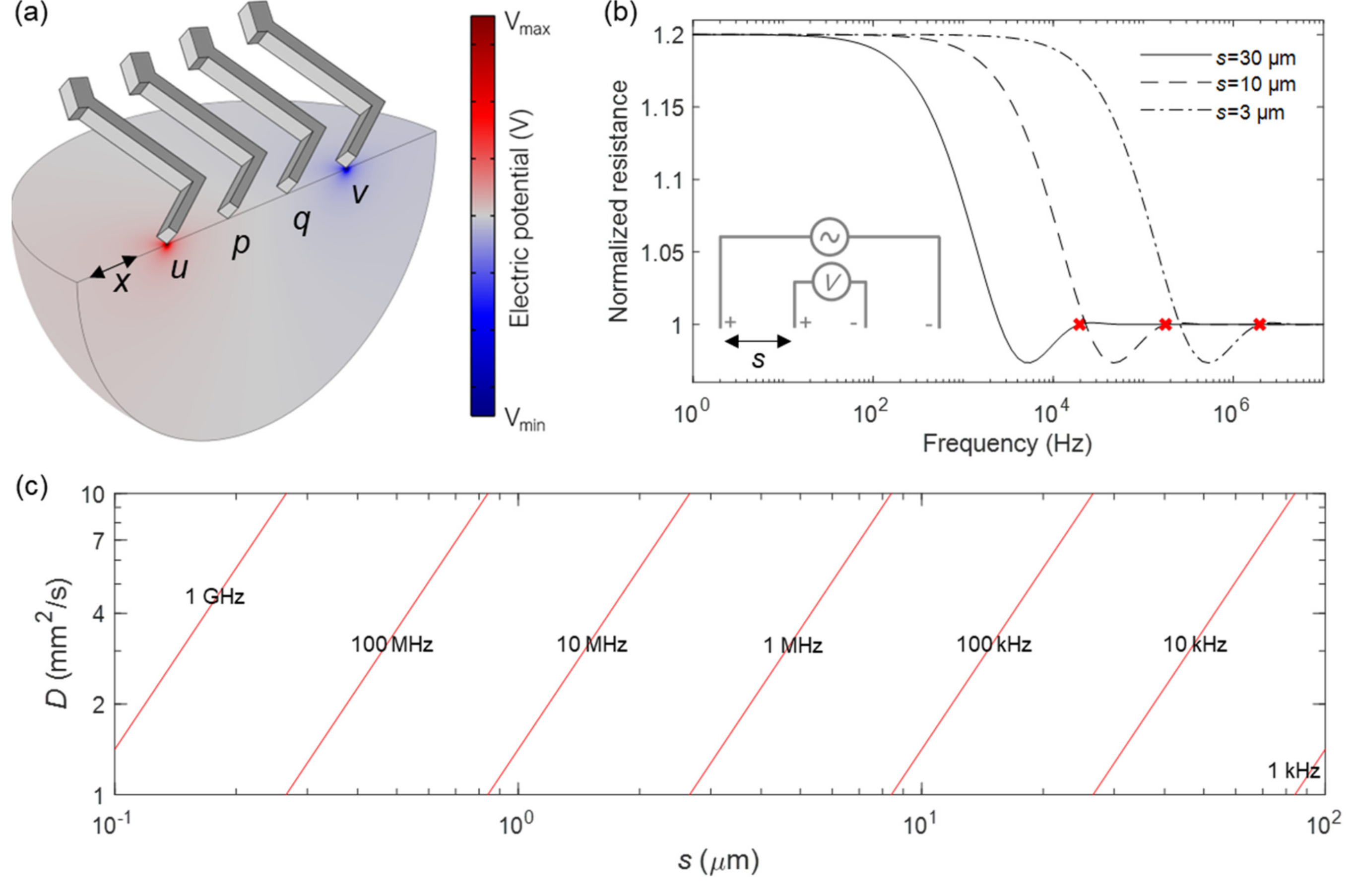

FIG. 1. (a) Schematic (not to scale) of the setup used in this study with visualization of the electric potential when current is injected at pin u and extracted at pin v. The arrow indicates the probe direction. (b) Normalized resistance simulations using Eqs. (1) and (3) of a material with a thermal diffusivity of $D = 2.5\,\text{mm}^2/\text{s}$ and a correction factor $C = 0.2$. The red crosses indicate the cutoff frequency f_c. (c) Simulations of f_c for different values of s and D.

08 January 2025 14:24:06

(σ_{eff} and C) can be determined simultaneously by fitting the resistance values of a frequency sweep even when the high-frequency limit is not reached. This strategy can reduce the need for measuring at high frequencies by as much as two orders of magnitude [see Fig. 1(b)].

III. EXPERIMENTAL SETUP

Three samples were used in this study, two skutterudites (one n-type $CoSb_{2.75}Sn_{0.05}Te_{0.20}$ and the other p-type $Ce_{0.5}Yb_{0.5}Fe_{3.25}Co_{0.75}Sb_{12}$) and a bismuth telluride (a p-type Bi_2Te_3). The skutterudites, which are isotropic and with a small grain size (ca. 150 nm), were prepared as explained in Ref. 24. Bismuth telluride, which was used in a previous study,[13] is anisotropic and with a grain size of hundreds of μm. Due to its anisotropic nature, measurements for the bismuth telluride material were conducted with the pins both (i) perpendicular and (ii) parallel to the c-axis of the crystal. This was possible since the c-axis of each grain in the bismuth telluride sample was determined by electron backscatter diffraction (EBSD). The EBSD results can be found in the supplementary information of Ref. 13. In total, four sets of data were collected, as labeled in Table I. Table I includes the values of thermal diffusivity in the probe direction (D_x), and the measured bulk consolidated pellet values for the electrical conductivity σ_m, Seebeck coefficient α_m, thermal conductivity κ_m, and dimensionless figure of merit ZT_m, which were determined as explained in the appendix. All M4PP measurements were performed with a CAPRES A301 microRSP® tool using a Ru-coated equidistant four-point probe with $s = 30\,\mu$m. Before the measurements, the samples were gently polished to decrease surface roughness.

IV. RESULTS AND DISCUSSION

For each of the four sets of data (see Table I), five frequency scans (3, 6, 12, 24, 48, 96, 193, and 386 Hz) at 1.5 mA RMS current were performed. A representative frequency scan of each dataset (circles) is shown in Figs. 2(a)–2(d) together

© Author(s) 2024

TABLE I. Description of the four sets of data used in this study, including the material, measuring direction, thermal diffusivity in the probe direction, and bulk consolidated pellet reference data at room temperature.

Name	Material	Measuring direction	D_x (mm^2/s)	σ_m (S/mm)	α_m (μV/K)	κ_m (W/m K)	ZT_m
Skut-1	$CoSb_{2.75}Sn_{0.05}Te_{0.20}$	N/A (isotropic)	2.26 ± 0.17	105	−140	4.7	0.13
Skut-2	$Ce_{0.5}Yb_{0.5}Fe_{3.25}Co_{0.75}Sb_{12}$	N/A (isotropic)	1.53 ± 0.22	161	80	3.1	0.10
Bi_2Te_3-1	Bi_2Te_3	Perpendicular to c-axis	1.57 ± 0.04	56.3	180	1.25	0.43
Bi_2Te_3-2	Bi_2Te_3	Parallel to c-axis	0.72 ± 0.03	56.3	180	1.25	0.43

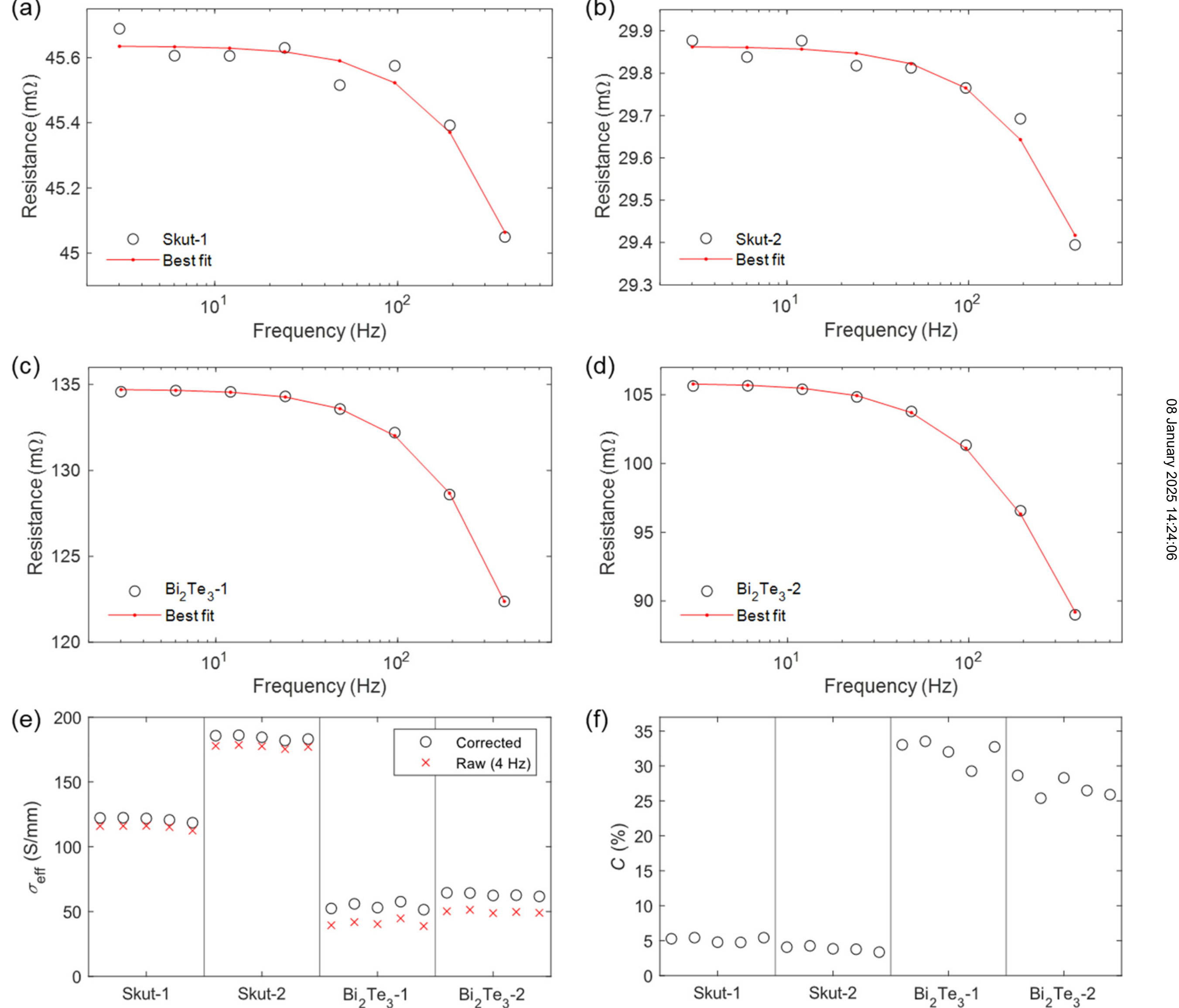

FIG. 2. (a)–(d) show the experimental M4PP resistance values (symbols) from a single measurement with their respective best fits (curves) obtained with MATLAB by fitting simultaneously σ_{eff} and C, which are shown (for each of the five frequency scans) in (e) and (f), respectively. The fitting uncertainty of the σ_{eff} values in (e), estimated from the covariance matrix, was mostly below 0.5%.

08 January 2025 14:24:06

© Author(s) 2024

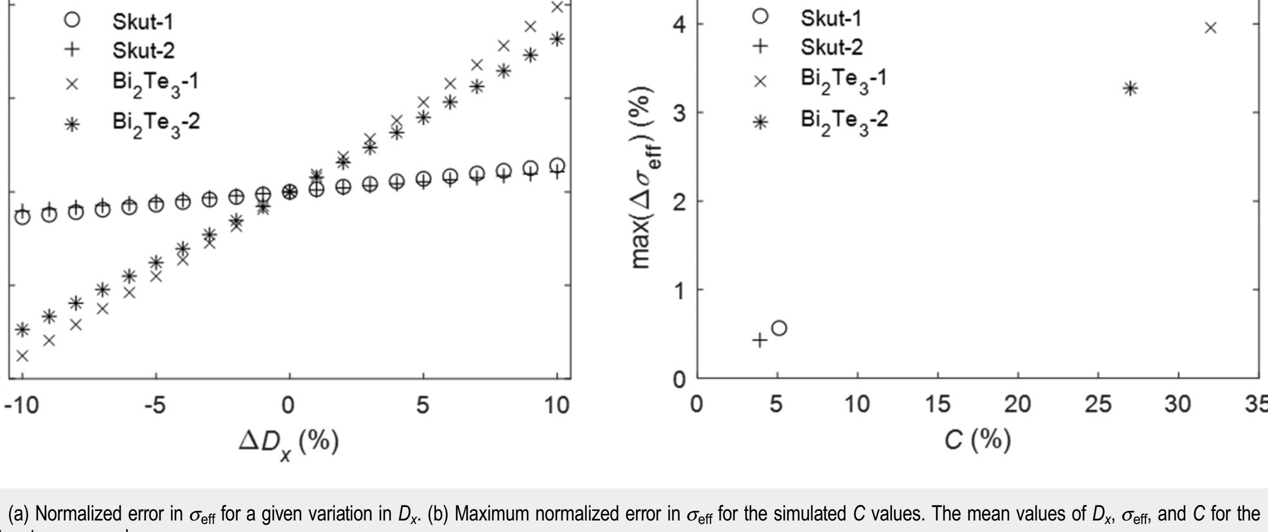

FIG. 3. (a) Normalized error in σ_{eff} for a given variation in D_x. (b) Maximum normalized error in σ_{eff} for the simulated C values. The mean values of D_x, σ_{eff}, and C for the four datasets were used.

with the best-fit values (lines) calculated with MATLAB using Eq. (1). All fittings were performed with the nominal pin positions, which is appropriate considering that the electrode separation is much larger than the position uncertainty.[7] When using smaller probes, experimental determination of the pin positions to increase the measurement precision must be considered.[7] Two parameters were fitted simultaneously, σ_{eff} and C, which can be found in Figs. 2(e) and 2(f), respectively, while keeping D_x fixed to the value calculated from the second harmonic phase (see Table I). The possibility of performing the fitting with the three parameters (D_x, σ_{eff}, and C) as free variables was also considered. However, this procedure was only successful for the Bi_2Te_3-2 dataset. This is not surprising considering that it is the dataset with the lowest D_x and hence, the decay in resistance appears at lower frequency values.[12] This dataset also shows the largest resistance drop, reducing the sensitivity to the equipment precision and facilitating fitting. Notice that the resistance drop is significantly different for each dataset, which is not evident due to the different scaling of Figs. 2(a)–2(d). Improving the measurement precision, increasing the number of frequency points, or measuring higher frequencies may avoid the need to provide D_x. It is worth mentioning that the possibility of the M4PP resistance being affected by the temperature coefficient of resistance was discarded due to the low magnitude of the recorded third harmonic signal (around 0.1% of the first harmonic). More information can be found in Ref. 25. It also discarded the possibility of the trends in Figs. 2(a)–2(d) being artifacts since the load resistances in all samples were similar and frequency independent, while the resistance drop of each dataset was significantly different.

The fitted mean σ_{eff} values were 121.1 ± 1.6, 184.3 ± 1.7, 54.1 ± 2.6, and 63.1 ± 1.2 S/mm for the datasets Skut-1, Skut-2, Bi_2Te_3-1, and Bi_2Te_3-2, respectively [see Fig. 2(e)]. As expected, the fitted values are larger than the raw measured conductivities at the lowest frequency (4 Hz), which are also plotted in Fig. 2(e) for comparison (red crosses). The percentages of resistance overestimation (given by the fitted C values) are plotted in Fig. 2(f). In all cases, the C values are significantly lower than the measured ZT_m (see Table I), indicating that a large portion of the Peltier-generated heat is dissipated toward the current pins, which increases the difficulty of measuring thermoelectric properties. It should be remarked that $C = ZT_m$ is only expected for homogeneous isotropic samples under perfect adiabatic conditions, and determining ZT locally assuming these conditions are met could result in a large measuring error. For the samples studied, it was found that performing measurements at low frequencies can produce overestimates of the measured resistance of up to 35% [see Fig. 2(f)]. It should be noted that C values can vary simply by changing the probe and, in general, larger C values are expected for higher performing thermoelectric materials.

A sensitivity analysis in the determination of σ_{eff} due to the uncertainty in D_x was performed for the four datasets as shown in Fig. 3(a). Four simulations with the mean values of D_x, σ_{eff}, and C were performed, which were fitted in the same way as the experimental data. Therefore, the data were fitted with σ_{eff} and C as free variables while fixing 21 different values of D_x for each dataset [Fig. 3(a)]. The variation in σ_{eff} was calculated to be up to 4% for the Bi_2Te_3-1 dataset when the fixed D_x was 10% larger than the nominal value [see Fig. 3(a)]. Finally, the maximum variation in σ_{eff} of each dataset (obtained when D_x was overestimated 10%) was plotted against the simulated C, see Fig. 3(b). The results indicate that even in this case with large uncertainty in D_x, the accuracy in the measured σ_{eff} is improved by an order of magnitude compared to the conductivity measured in the low-frequency limit.

08 January 2025 14:24:06

© Author(s) 2024

V. CONCLUSIONS

When measuring thermoelectric materials by M4PP, a Seebeck voltage (in addition to the ohmic voltage) is recorded due to the Peltier effect producing a temperature difference between the voltage reading pins. This voltage is difficult to quantify due to thermal losses, mainly toward the current pins. Measuring at sufficiently high frequencies can remove this unwanted contribution, but this is particularly challenging due to the small separation between the pins of the probe. The issue escalates as separation and probe size are decreased (potentially extending the high-frequency limit into the GHz region) to enhance spatial resolution. The theoretical model developed in this study can be used to model the voltage reading. Since typical M4PP measurements cannot reach the high-frequency limit, the model can also be used to fit experimental data at lower frequencies and obtain σ_{eff} (free of error due to the Peltier effect) by a fitting procedure. This is demonstrated for three dissimilar materials, two isotropic skutterudites (Skut-1 and Skut-2) and a bismuth telluride that was measured perpendicular and parallel to the c-axis (Bi_2Te_3-1 and Bi_2Te_3-2). Theoretically, all three parameters that define the voltage can be fitted simultaneously (D_x, σ_{eff}, and C); however, this proved challenging due to the comparatively narrow range of frequencies available in our setup. Fortunately, the second harmonic phase shift can be used to calculate D_x, as we have recently demonstrated. Then, D_x can be fixed in our fitting model to leave only two free parameters (σ_{eff} and C). A sensitivity analysis reveals that the accuracy in σ_{eff} significantly improves, with respect to conventional M4PP measurements, even when the uncertainty in D_x is large. In our samples, the error in σ_{eff} when not accounting for thermoelectric effects, given by the C value, was found to be up to 35% for the Bi_2Te_3-1 dataset, demonstrating the need of such correction. Furthermore, the C values are significantly lower than the expected ZT_m, which is attributed to a sizable portion of the Peltier-generated heat being dissipated toward the current pins. Since the C values are not just a material property, and they may change due to external factors such as using a different probe type, it is considered difficult to use them for measuring thermoelectric properties such as the ZT.

SUPPLEMENTARY MATERIAL

See the supplementary material for the reasoning behind the selection of the cutoff frequency, f_c.

ACKNOWLEDGMENTS

The authors acknowledge financial support from Innovation Fund Denmark for the Industrial Postdoc 1045-00029B, the Independent Research Fund Denmark (Grant No. 8048-00088B), and the EliteForsk travel (Grant No. 2083-00010B). J.P.G. acknowledges MCIU/AEI/10.13039/501100011033 and the European Union Next Generation EU/PRTR for funding the projects TED2021-129569A-I00 and CNS2022-135302. Yaron Amouyal from Technion is thanked for supporting the external stay during the preparation of the Bi_2Te_3 sample. The technician Ebtisam Abdellahi is also acknowledged for polishing the samples.

AUTHOR DECLARATIONS

Conflict of Interest

The authors have no conflicts to disclose.

Author Contributions

Neetu Lamba: Data curation (equal); Investigation (equal); Methodology (equal); Software (equal); Writing – original draft (equal). **Benny Guralnik:** Data curation (equal); Methodology (equal); Resources (equal); Validation (equal); Writing – review & editing (equal). **Jesús Prado-Gonjal:** Investigation (equal); Resources (equal); Writing – review & editing (equal). **Anthony V. Powell:** Funding acquisition (equal); Investigation (equal); Resources (equal); Supervision (equal); Writing – review & editing (equal). **Nini Pryds:** Funding acquisition (equal); Project administration (equal); Resources (equal); Writing – review & editing (equal). **Ole Hansen:** Formal analysis (equal); Investigation (equal); Methodology (equal); Supervision (equal); Validation (equal); Writing – review & editing (equal). **Dirch H. Petersen:** Funding acquisition (equal); Project administration (equal); Resources (equal); Supervision (equal); Validation (equal); Writing – review & editing (equal). **Braulio Beltrán-Pitarch:** Conceptualization (equal); Data curation (equal); Formal analysis (equal); Investigation (equal); Methodology (equal); Supervision (equal); Validation (equal); Visualization (equal); Writing – review & editing (equal).

DATA AVAILABILITY

The data that support the findings of this study are available from the corresponding author upon reasonable request.

APPENDIX: EXPLANATION OF THE THERMAL AND THERMOELECTRIC PROPERTIES CHARACTERIZATION USED AS REFERENCE MACROSCOPIC VALUES

The values of σ_m and α_m shown in Table I were determined simultaneously (using a Linseis LSR3-800 for the skutterudites and a Netzsch SBA for the bismuth telluride), while κ_m of the pellets was measured with the commonly used laser flash method (using a Netzsch LFA system). Assuming a room temperature of $T = 298$ K, the bulk $ZT_m = \sigma_m \alpha_m{}^2 T/\kappa_m$ values were calculated. Finally, the D_x of each dataset was obtained from the second harmonic phase shift of M4PP measurements using the CAPRES A301 microRSP® tool as explained in detail in Ref. 13, and it can be summarized as follows.

When measuring on an isotropic 3D sample, the second harmonic voltage difference ${}^{uv}_{pq}\Delta V_{2\omega}$ between pin p and pin q due to a current introduced at pin u and removed at pin v [see Fig. 1(a)] can be expressed as[12]

$$ {}^{uv}_{pq}\Delta V_{2\omega} = -\alpha({}^{u}_{p}\Delta T_{2\omega} + {}^{v}_{p}\Delta T_{2\omega} - {}^{u}_{q}\Delta T_{2\omega} - {}^{v}_{q}\Delta T_{2\omega}), \tag{A1} $$

where ${}^{l}_{k}\Delta T_{2\omega}$ is the rise in temperature at pin k due to Joule heating at pin l and α is the Seebeck coefficient. The second harmonic

08 January 2025 14:24:06

© Author(s) 2024

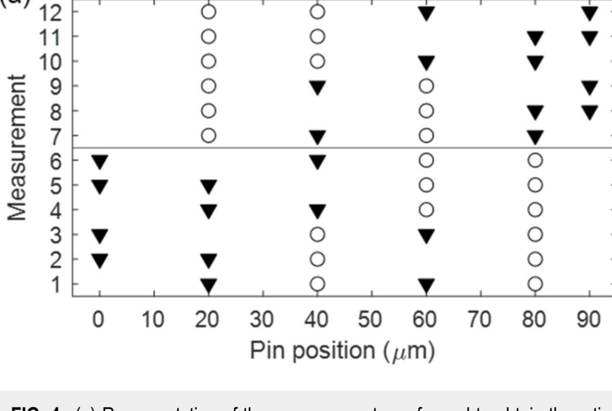

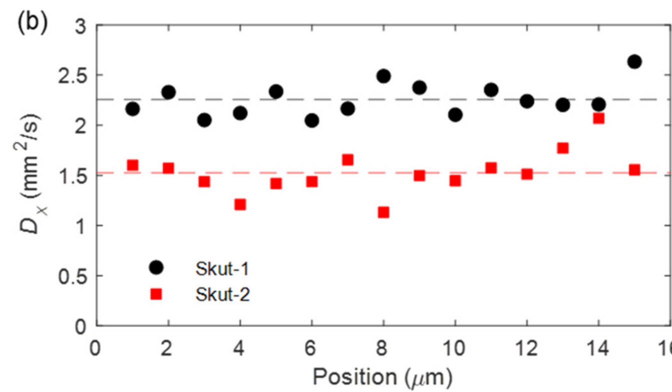

FIG. 4. (a) Representation of the measurements performed to obtain the ratio Γ_1. The black triangles represent current pins while the empty circles indicate the position of the voltage reading. (b) Thermal diffusivity for the skutterudites used in this study. The dashed lines indicate the mean of each sample.

temperature ${}^{l}_{k}\Delta T_{2\omega}$ can be defined as

$$ {}^{l}_{k}\Delta T_{2\omega}(r_{k,l}, t) = \frac{I_{rms}^2 R_{c,l}}{2\pi\kappa r_{k,l}} e^{-(1+i)\sqrt{\frac{\omega}{D}} r_{k,l}} e^{2i\omega t}, \tag{A2} $$

where $r_{k,l}$ is the separation between pin k and pin l, t is the time, I_{rms} is the root mean squared current, $R_{c,l}$ is the electrical contact resistance of pin l, κ is the thermal conductivity, ω is the angular frequency, i is the imaginary unit, and D is the thermal diffusivity.

For simplicity, a probe with five pins labeled 1 to 5 can be considered, and the second harmonic voltage difference given by Eq. (A1) of six measurements can be combined to define the ratio Γ_1 as[13]

$$ \Gamma_1 = \frac{{}^{13}_{24}\Delta V_{2\omega} + {}^{15}_{24}\Delta V_{2\omega} - {}^{35}_{24}\Delta V_{2\omega}}{{}^{12}_{34}\Delta V_{2\omega} + {}^{15}_{34}\Delta V_{2\omega} - {}^{25}_{34}\Delta V_{2\omega}}. \tag{A3} $$

After a few algebraic steps, the constants α, I_{rms}, $R_{c,l}$, and κ cancel, and D becomes the only unknown material property,

$$ \Gamma_1 = \frac{{}^{1}_{2}\Delta T_{2\omega} - {}^{1}_{4}\Delta T_{2\omega}}{{}^{1}_{3}\Delta T_{2\omega} - {}^{1}_{4}\Delta T_{2\omega}} = \frac{\dfrac{e^{-(1+i)\sqrt{\frac{\omega}{D}} r_{2,1}}}{r_{2,1}} - \dfrac{e^{-(1+i)\sqrt{\frac{\omega}{D}} r_{4,1}}}{r_{4,1}}}{\dfrac{e^{-(1+i)\sqrt{\frac{\omega}{D}} r_{3,1}}}{r_{3,1}} - \dfrac{e^{-(1+i)\sqrt{\frac{\omega}{D}} r_{4,1}}}{r_{4,1}}}. \tag{A4} $$

Notice that in the case of anisotropic samples, the thermal diffusivity (D) appearing in Eq. (A4) is the thermal diffusivity in the probe direction (D_x).[13]

As shown in Eq. (A3), a minimum of six measurements are required to obtain a D_x value. Experimentally, 12 measurements were performed, which are represented by each row in Fig. 4(a). To reproduce the procedure described in Ref. 13, the first two Γ_1 values were calculated [using measurements 1–6 and 7–12 of Fig. 4(a)], and then, the mean of both values was used to obtain a single D_x using Eq. (A4). These steps were repeated at 15 locations on each skutterudite sample as shown in Fig. 4(b), and the mean values are shown in Table I. The values of D_x found in Table I for the bismuth telluride sample are already reported in Ref. 13.

REFERENCES

[1]I. Miccoli, F. Edler, H. Pfnür, and C. Tegenkamp, J. Phys.: Condens. Matter **27**, 223201 (2015).
[2]C. L. Petersen, T. M. Hansen, P. Bøggild, A. Boisen, O. Hansen, T. Hassenkam, and F. Grey, Sens. Actuators, A **96**(1), 53–58 (2002).
[3]A. Uhlir, Bell. Syst. Techn. J. **34**(1), 105–128 (1955).
[4]S. Thorsteinsson, F. Wang, D. H. Petersen, T. M. Hansen, D. Kjær, R. Lin, J.-Y. Kim, P. F. Nielsen, and O. Hansen, Rev. Sci. Instrum. **80**(5), 053902 (2009).
[5]D. H. Petersen, O. Hansen, R. Lin, and P. F. Nielsen, J. Appl. Phys. **104**, 013710 (2008).
[6]D. C. Worledge and P. L. Trouilloud, Appl. Phys. Lett. **83**(1), 84–86 (2003).
[7]A. Cagliani, F. W. Østerberg, O. Hansen, L. Shiv, P. F. Nielsen, and D. H. Petersen, Rev. Sci. Instrum. **88**(9), 095005 (2017).
[8]T. A. Marangoni, B. Guralnik, K. A. Borup, O. Hansen, and D. H. Petersen, J. Appl. Phys. **129**(16), 165105 (2021).
[9]B. Beltrán-Pitarch, B. Guralnik, K. A. Borup, C. Adelmann, O. Hansen, N. Pryds, and D. H. Petersen, Meas. Sci. Technol. **35**(6), 066012 (2024).
[10]B. Guralnik, O. Hansen, A. R. Stilling-Andersen, S. E. Hansen, K. A. Borup, B. M. Mihiretie, B. Beltrán-Pitarch, H. H. Henrichsen, R. Lin, L. Shiv, B. B. Iversen, P. F. Nielsen, and D. H. Petersen, Meas. Sci. Technol. **33**, 125001 (2022).
[11]N. Lamba, B. Guralnik, B. Beltrán-Pitarch, V. Rosendal, N. Pryds, O. Hansen, and D. H. Petersen, Int. J. Therm. Sci. **196**, 108716 (2024).
[12]B. Beltrán-Pitarch, B. Guralnik, N. Lamba, A. R. Stilling-Andersen, L. Nørregaard, T. M. Hansen, O. Hansen, N. Pryds, P. F. Nielsen, and D. H. Petersen, Mater. Today Phys. **31**, 100963 (2023).
[13]N. Lamba, B. Beltrán-Pitarch, T. Yu, M. Dawod, A. Berner, B. Guralnik, A. Orekhov, N. Gauquelin, Y. Amouyal, J. Verbeeck, O. Hansen, N. Pryds, and D. Petersen, PREPRINT (Version 1) available at Research Square https://doi.org/10.21203/rs.3.rs-4178322/v1 (2024).
[14]T. C. Harman, *Special Techniques for Measurement of Thermoelectric Properties* (1958), Vol. 29, pp. 1373–1374.
[15]I. J. Roh, Y. G. Lee, M. S. Kang, J. U. Lee, S. H. Baek, S. K. Kim, B. K. Ju, D. B. Hyun, J. S. Kim, and B. Kwon, Sci. Rep. **6**, 39131 (2016).

08 January 2025 14:24:06

© Author(s) 2024

[16]M. S. Kang, I. J. Roh, Y. G. Lee, S. H. Baek, S. K. Kim, B. K. Ju, D. B. Hyun, J. S. Kim, and B. Kwon, Sci. Rep. **6**, 26507 (2016).
[17]B. Beltrán-Pitarch, J. Prado-Gonjal, A. V. Powell, P. Ziolkowski, and J. García-Cañadas, J. Appl. Phys. **124**(2), 025105 (2018).
[18]B. Beltrán-Pitarch, J. Prado-Gonjal, A. V. Powell, F. Martínez-Julián, and J. García-Cañadas, J. Phys. Chem. C **123**(20), 12608–12613 (2019).
[19]T. Arisaka, M. Otsuka, and Y. Hasegawa, Rev. Sci. Instrum. **90**, 46104 (2019).
[20]M. Otsuka, T. Arisaka, and Y. Hasegawa, Mater. Sci. Eng. B **261**, 114620 (2020).
[21]K. Okawa, Y. Amagai, H. Fujiki, and N. H. Kaneko, Commun. Phys. **4**(1), 267 (2021).
[22]K. Okawa, Y. Amagai, N. Sakamoto, and N. H. Kaneko, Measurement **232**, 114626 (2024).
[23]B. Beltrán-Pitarch, J. Prado-Gonjal, A. V. Powell, and J. García-Cañadas, J. Appl. Phys. **125**, 025111 (2019).
[24]J. Prado-Gonjal, M. Phillips, P. Vaqueiro, G. Min, and A. V. Powell, ACS Appl. Energy Mater. **1**(11), 6609–6618 (2018).
[25]B. Guralnik, O. Hansen, H. H. Henrichsen, B. Beltrán-Pitarch, F. W. Østerberg, L. Shiv, T. A. Marangoni, A. R. Stilling-Andersen, A. Cagliani, M. F. Hansen, P. F. Nielsen, H. Oprins, B. Vermeersch, C. Adelmann, S. Dutta, K. A. Borup, B. M. Mihiretie, and D. H. Petersen, Rev. Sci. Instrum. **92**(9), 094711 (2021).

08 January 2025 14:24:06

© Author(s) 2024